THE JOURNAL OF PHYSICAL CHEMISTRY A

Article

pubs.acs.org/JPCA

Correlated Dynamics of the O(^{3}P) + CHD$_3$(v=0) Reaction: A Joint Crossed-Beam and Quasiclassical Trajectory Study

Bailin Zhang,[†,§] Kopin Liu,*[,†] and Gábor Czakó*[,‡]

[†]Institute of Atomic and Molecular Sciences (IAMS), Academia Sinica, P.O. Box 23-166, Taipei, Taiwan 10617

[‡]Laboratory of Molecular Structure and Dynamics, Institute of Chemistry, Eötvös University, P.O. Box 32, H-1518 Budapest 112, Hungary

ABSTRACT: Crossed beam experiments and quasiclassical trajectory computations on an *ab initio* potential energy surface are performed for the O(^{3}P) + CHD$_3$(v=0) → OH(v'=0) + CD$_3$(v_2=0,2) and OD(v'=0,1) + CHD$_2$(v=0) reactions. Both experiment and theory show that the excitation functions display a concave-up behavior and the angular distributions are backward scattered, indicating a direct rebound mechanism and a tight-bend transition state. The reaction produces mainly ground-state products showing the dominance of a vibrationally adiabatic reaction pathway. The standard histogram binning cannot reproduce the observed vibrational adiabaticity, whereas Gaussian binning gives good agreement with experiment.

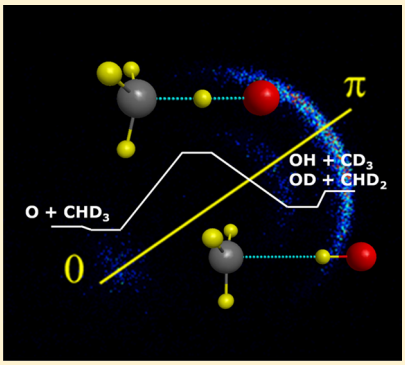

I. INTRODUCTION

The abstraction reaction of O(^{3}P) + CH$_4$ is an important initial step in hydrocarbon combustion.[1] Its thermal kinetics has been extensively investigated, both experimentally[2] and theoretically,[3−5] over the past decades. The recommended experimental rate constant for the temperature range 300−2500 K can be expressed as $k = 1.15 \times 10^{-15} T^{1.56} \exp(-4720/T)$ cm^3 molecule^{-1} s^{-1}.[2] Two most recent theoretical calculations,[4,5] based on accurate *ab initio* potential energy surfaces (PESs),[6,7] showed excellent agreement with the above expression. The reaction is slightly endothermic by 1.59 kcal mol^{-1} with a substantial adiabatic barrier to reaction, ∼10 kcal mol^{-1}. Although the high barrier and the high dimensionality (12 degrees of freedom) of this six-atom reaction pose considerable challenges to detailed dynamics studies from the experimental and theoretical perspectives, respectively, significant progress has been made in recent years.

On the experimental side, earlier dynamics studies focused on the product-state distributions of the ground-state reaction. The key observations can be summarized as follows. (1) The vibrational distribution in the umbrella mode of CH$_3$ products declines monotonically from v = 0 to v_2 = 4,[8] suggesting that the CH$_3$ moiety is gradually relaxed to a planar structure during the course of reaction. (2) The OH(v'=0) rotational distribution is relatively cold,[9] consistent with the theoretical prediction of an abstraction mechanism with a preferentially collinear O−H−C transition-state geometry.[3−5] The renewed interest in the dynamics studies of this reaction was arguably sparked by the development of correlated angular and vibrational product distribution measurements.[10−14] In particular, the report on the CH-stretch excited CHD$_3$(v_1=1) reaction with O(^{3}P)[15] inspired a number of theoretical studies[16−23] and a followed up experiment,[24] focusing on the issues of the effects of reagents vibrations on reactivity and of the possible extension of the Polanyi's rule[25] to this central-barrier polyatomic reaction.

Recent theoretical advances in dynamics of this reaction are triggered by two newly developed, full dimensional *ab initio* PESs.[7,16] Either quasiclassical trajectory (QCT) or reduced dimensionality quantum dynamics (QD) calculations have been performed using these PESs and compared with available experimental results.[16−23] On the one hand, due to computational difficulties, the reported QD results are limited only to the total reaction cross sections. On the other hand, QCT can provide the (correlated) product angular and state distributions, subject to the usual problems of quantum effects such as tunneling and the zero-point energy (ZPE) issues. In all cases, reasonably good agreements between theory and experiment are found, demonstrating the accuracy of the PESs and confirming the direct abstraction reaction mechanism. Most of theoretical results so far are, however, on the O(^{3}P) + CH$_4$/CD$_4$ reactions, except for two recent reports.[16,20] Using a 6-dimensional QD approach, Yan et al. computed the excitation functions for both the vibrationally excited and ground-state O(^{3}P) + CHD$_3$ → OH + CD$_3$ reactions, which showed good agreements with experimental findings.[20] Using the QCT approach, Czakó and Bowman calculated the pair-correlated

Special Issue: 100 Years of Combustion Kinetics at Argonne: A Festschrift for Lawrence B. Harding, Joe V. Michael, and Albert F. Wagner

Received: October 15, 2014
Revised: November 30, 2014
Published: December 2, 2014

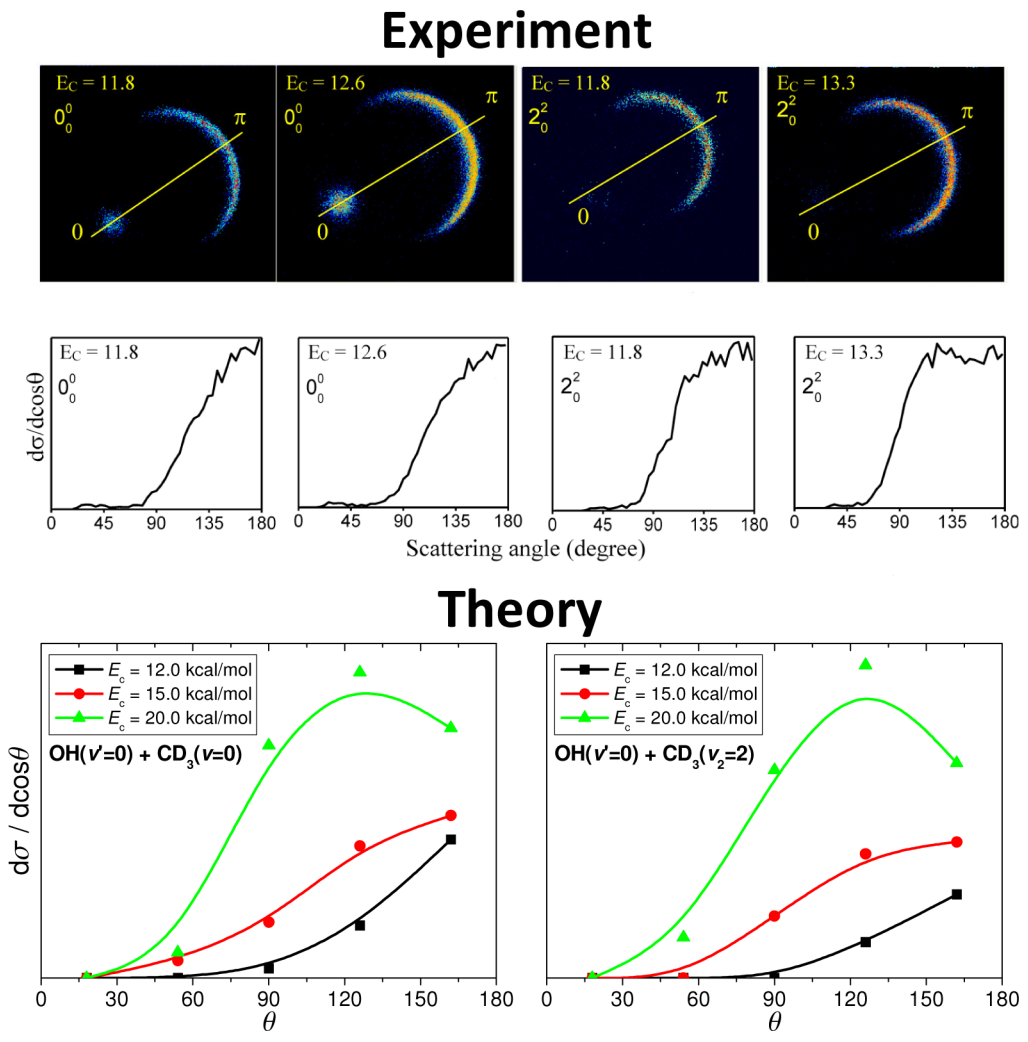

Figure 1. Four unnormalized raw images are exemplified in the upper panel, the left two for the ground-state $CD_3(v=0)$ products and the right two for the umbrella-mode, first-overtone excitation of $CD_3(v_2=2)$. The forward scattering angle 0° denotes the initial CHD_3 direction in the center-of-mass collision frame. Some photolysis generated backward in the forward direction was seen and discarded in image analysis. The resultant correlated angular distributions for the $OH(v'=0)$ + $CD_3(v_2=0$ or 2) product pairs are presented in the middle panel. The computed correlated angular distributions at different collision energies are shown in the lower panel.

differential cross sections (DCS) in the $O(^3P)$ + $CHD_3(v_1=0,1)$ → $OH(v'=0)$ + $CD_3(v=0)$ reactions, at a single collision energy (E_c) of 11.4 kcal mol^{-1}.[16] Excellent agreement with experiment was found, and the detailed theoretical analysis confirmed the experimental conjecture that the vibrational enhancement in reactivity is primarily due to opening the cone-of-acceptance.[15]

Encouraged by those fragmentary theory−experiment agreements, it is desirable to have a more extensive comparison. Reported here is a joint theory and experiment study of the ground-state reaction of $O(^3P)$ + $CHD_3(v=0)$ over an extended collision energy range. In addition, both isotopic product channels, $OH(v'=0)$ + $CD_3(v=0)$ and $OD(v'=0, 1)$ + $CHD_2(v=0)$, as well as an umbrella-excited product pair $OH(v'=0)$ + $CD_3(v_2=2)$ are examined for the first time.

II. EXPERIMENTAL METHOD

The rotating-sources, crossed-beam apparatus, and the time-sliced velocity-map imaging technique for interrogating the product pair-correlated angular distributions have been described previously.[13−15,24,26] Only the relevant features are presented here. The $O(^3P)$-atom beam was generated by photolyzing SO_2 (4−5% seeded in H_2 at total pressure of 12 atm) by an excimer laser at 193 nm near the throat of a PZT (piezoelectric translator) pulsed valve.[13,14] To remove the small chemical interferences from the reaction of the OH byproduct in the beam (as evidenced from the recorded images that were contaminated by some fait features nearly identical to those reported in refs 27 and 28), the ArF laser was loosely focused into a Teflon block, which was attached to the pulsed valve, to deactivate the trace amounts of the $O(^1D)$ radical that is thought to be the precursor for the OH contaminants in the beam. Using a similar setup, previous studies demonstrated that most of O atoms (~98%) were supersonically cooled to the lowest fine-structure state $O(^3P_2)$.[29,30] Because of the high barrier to reaction, the CHD_3 beam was also seeded (~20%) in H_2 for acceleration. To investigate the initial translational energy dependence of the reactivity, the intersection angle of the two molecular beams was varied, thereby changing the relative collision energy in the center-of-mass frame. Due to the presence of a copious amount of photolyzed $S(^3P)$ atoms in the beam and the difference of the reduced masses for $O(^3P)$ + CHD_3 and $S(^3P)$ + CHD_3, this study is limited to the E_c range from ~7.5 to 13.5 kcal mol^{-1}. [The methyl radical signals from

dx.doi.org/10.1021/jp510377k | J. Phys. Chem. A 2015, 119, 7190−7196

$S(^3P)$ + CHD_3 started to kick in at $E_c \sim 20$ kcal mol^{-1}. At that intersection angle and beam speeds, the corresponding E_c for the $O(^3P)$ + CHD_3 reaction is about 14 kcal mol^{-1}.]

The reaction products $CD_3(v_2=0$ and 2) and $CHD_2(v=0)$ were detected by (2+1) resonance-enhanced multiphoton ionization (REMPI)[31] and recorded by time-sliced ion velocity-mapped images.[26] The laser frequencies of the probe were fixed at the respective peaks of the 0_0^0 and 2_2^0 Q-heads of the $3p_z\,^2A_2 \leftarrow X^2A_2$ transitions.[31−34] As a result, only the low N-states (N = 0−6) of methyl radical products were sampled. Nevertheless, the acquired REMPI spectra indicated that they represented the majority of the total reactivity of a given product vibration state. QCT calculations at three different collision energies, from 12 to 20 kcal mol^{-1}, showed a slight increase in the rotational excitation of methyl products with E_c. In consistence with the experimental suggestion, at E_c = 12 kcal mol^{-1} these low N-states account for, respectively, about two-third of the yields for the $OH(v'=0)$ + CD_3(all v states) channel and more than half of the $OD(v'=0)$ + CHD_2(all v states) product populations.

III. THEORETICAL CALCULATIONS

Full-dimensional QCT computations have been performed for the $O(^3P)$ + $CHD_3(v=0)$ reaction using the Czakó−Bowman *ab initio* PES.[16] The initial conditions are the same as in ref 16. In brief, standard normal-mode sampling is employed to prepare the quasiclassical vibrational ground state of CHD_3. The initial distance between the center of mass of the reactants is $(x^2 + b^2)^{1/2}$, where b is the impact parameter and x = 10 bohr. The orientation of CHD_3 is randomly sampled and b is scanned from 0 to 5 bohr with a step size of 0.5 bohr. We run 25 000 trajectories at each b; thus, the total number of trajectories is 275 000 for each E_c. QCT computations are carried out at six different collision energies in the E_c range 10−20 kcal mol^{-1}. We use an integration step of 0.0726 fs (3 atomic-unit-of-time) and the trajectories are propagated until the actual maximum interatomic distance is 1 bohr larger than the initial one.

To make direct comparison between theory and experiment, we have computed the cross sections and angular distributions corresponding to the $OH(v'=0)$ + $CD_3(v_2=0$ and 2) and $OD(v'=0,1)$ + $CHD_2(v=0)$ product channels. The correlated product vibrational states are assigned by employing the procedures described in refs 35 and 36. Cross sections are computed using both the standard histogram binning (HB) and the energy-based Gaussian binning (1GB).[35−37] 1GB assigns a weight to each reactive trajectory on the basis of the energy difference between the harmonic quantum vibrational energy of the product state and the actual classical vibrational energy of the product molecule obtained exactly in the Cartesian space.[36] In the case of a correlated product state, we compute a weight for each product and then calculate the product of the two weights, thereby accounting for any unphysical energy flow between the product molecules. Because 1GB gives small weights to trajectories that significantly violate ZPE, 1GB handles the usual ZPE issue of the QCT method. (Strictly speaking 1GB treats the ZPE violation of the total vibrational energy, but mode-specific ZPE violation is possible.) Note, however, that 1GB may not provide realistic absolute cross sections due to the "denominator issue". In the present study the reaction probabilities are obtained as the sum of weights of the reactive trajectories divided by the total number of trajectories. Thus, in the denominator we do not use the sum of weights of all the trajectories, because the assignment of realistic weights for nonreactive trajectories is problematic. (This could result in erroneously large weights for some of the nonreactive trajectories, especially at high b, where the interaction between the reactants may be small. Further discussion and possible solutions of the 1GB normalization issue can be found in ref 37.) Therefore, the 1GB cross sections should be considered in a relative scale. For the correlated angular distributions we use HB to ensure the good statistical accuracy.

IV. RESULTS AND DISCUSSION

A. OH(v'=0) + $CD_3(v_2$=0, 2) Channels. Figure 1 (upper panel) exemplifies four raw images, two for $CD_3(v=0)$ and two for $CD_3(v_2=2)$ products. All four images show a distinct backward-dominant feature corresponding to the $OH(v'=0)$ + $CD_3(v_2=0$ or 2) product pair. After the density-to-flux correction,[26,38] the pair-correlated angular distributions can be obtained and displayed in the lower experimental panel. As is seen, all distributions are sharply backward peaking, indicative of a direct rebound mechanism. A closer inspection reveals some subtle trends. For example, for a given CD_3 vibrational state, the increase in E_c broadens the angular distribution. Comparing the $CD_3(v_2=2)$ distribution to $CD_3(v=0)$ at similar E_c's shows the former is distinctly broader despite less available energy for disposal. Figure 1 also presents the corresponding QCT results over a much wider E_c range than experiment. The dominance of backward-scattered distributions is clearly reproduced; however, the subtle trends, i.e., the E_c- and the CD_3 vibrational-state dependences, are less obvious than experiment. Nevertheless, theory shows that the angular distributions shift toward sideways directions as E_c increases, in qualitative agreement with experiment. This shift suggests that the probability of the stripping mechanism (reactivity at larger impact parameters) slightly increases with E_c. Note that previously we found much more pronounced E_c-dependent backward−forward shift for the Cl + $CH_4(v=0)$ reaction,[39] indicating that the stripping mechanism is more significant in the Cl-atom reaction than in the $O(^3P)$-atom reaction.

Following the procedure described previously,[40] the pair-correlated excitation functions (i.e., the collision energy dependency of the integral cross sections) were obtained by normalizing the images at different E_c. Figure 2 upper panel presents the experimental results. Because we do not know the Franck−Condon factors of the 0_0^0 and 2_2^0 bands, the ordinates of the two experimental plots merely reflect the relative REMPI signal strengths. Both product states indicate a reactive threshold of ∼8 kcal mol^{-1}, which compares well to the previously reported value for $O(^3P)$ + CH_4 [ref 14] and to the theoretically predicted adiabatic barrier height of ∼10 kcal mol^{-1}.[7,16] The slight discrepancy in energy conceivably arises from the tunneling effects of the transferred H atom and/or theory may overestimate the adiabatic barrier. (Theoretically the classical barrier height is known accurately, 14.1 ± 0.2 kcal mol^{-1} without spin−orbit correction;[16] however, the apparently large vibrational effects on the barrier height have large uncertainties.) In the post-threshold region, both excitation functions display a distinct concave-up dependency, again similar to the observation for $O(^3P)$ + CH_4,[14] yet in sharp contrast to the concave-down behavior seen in the nearly isoenergetic Cl + $CHD_3(v=0)$ reaction.[41] As argued previously, such a concave-up dependency of excitation function is the result of a relatively tight-bend transition-state structure near the barrier.[14] The tight-bend conjecture is also in line with the

dx.doi.org/10.1021/jp510377k | J. Phys. Chem. A 2015, 119, 7190−7196

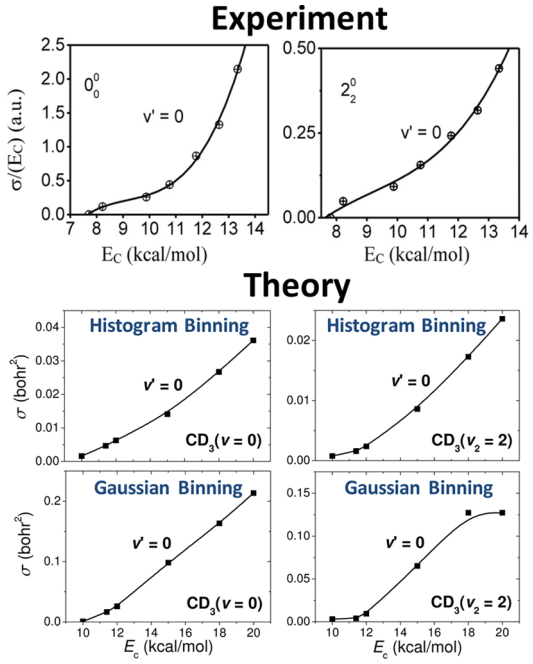

Figure 2. Experimental and theoretical excitation functions of the reactions $O(^3P) + CHD_3(v=0) \rightarrow OH(v'=0) + CD_3(v_2=0 \text{ and } 2)$. The ordinates of the two experimental plots, the left for $CD_3(v_2=0)$ and the right for $CD_3(v_2=2)$, are scaled according to the REMPI signal strengths. The QCT data are analyzed using different binning techniques. The absolute cross sections obtained by Gaussian binning (1GB) may not be realistic due to the normalization issue (see text for more details).

narrow angular range of the product angular distributions (Figure 1).

The corresponding QCT results obtained by HB and 1GB are also shown in Figure 2. As seen, both HB and 1GB display similar E_c dependencies and the concave-up behavior observed in the post-threshold region is well reproduced. 1GB gives significantly larger absolute cross sections, but this may not be realistic due to the normalization issue as mentioned in section III. The advantage of 1GB can be clearly seen in Figure 3, where the correlated OH vibrational branching ratios are shown at different E_c. In the experiment only $OH(v'=0)$ is observed, as expected on the basis of available energy. However, HB provides 20−40% populations for $OH(v'=1)$ due to the possible ZPE violation of CD_3 and the rounding issue of HB. As seen in Figure 3, 1GB solves these problems and provides physically correct results; i.e., the fraction of $OH(v'=1)$ drops to zero or close to zero at high E_c.

B. OD(v'=0, 1) + CHD$_2$(v=0) Channel. The upper experimental panel of Figure 4 illustrates two raw images when the $CHD_2(v=0)$ products are probed. Two distinct backward ring features are now seen, energetically corresponding to the concomitantly formed $OD(v'=0)$ and $OD(v'=1)$ products for the outer and inner rings, respectively. After the density-to-flux correction,[26,38] the desired correlated angular distributions (the middle experimental panel) and correlated OD vibrational distribution (the lower experimental panel) are presented. In contrast to the analogous $CD_3(v=0)$ channel (Figure 1), the change in E_c exerts little impact to the product angular distributions. From the recoil speed distributions (the lower experimental panel), it is clear that the $OD(v'=0)$ products dominate, indicative of a vibrationally adiabatic process. And this vibrational adiabaticity does not vary much with the change in E_c. For the $OD(v') + CHD_2(v)$ product channel, only the formation of the $CHD_2(v=0)$ product was reported here. [The signals for the $CHD_2(4_2^0)$ + OD product channel were also detected, but too weak to be quantified.] It is worth noting that the vibrationally adiabatic propensity also holds in the CH stretch-excited reaction of $O(^3P) + CHD_3(v_1=1)$,[15] for which about 90% of the OH products in the $OH(v') + CD_3(v=0)$ product channel are born in $v' = 1$—a highly inverted distribution. The computed $OD(v')$ vibrational branching ratios for $O(^3P) + CHD_3(v=0) \rightarrow OD(v'=0,1) + CHD_2(v=0)$ are shown in Figure 3. As seen, HB seriously overestimates $OD(v'=1)$, whereas 1GB gives only about 10% $OD(v'=1)$; i.e., the dominance of $OD(v'=0)$ is seen, in agreement with experiment.

Figure 4 also presents the computed angular distributions for the pair-correlated $OD(v'=0) + CHD_2(v=0)$ products and the center of mass speed distributions of $CHD_2(v=0)$. The angular distributions over the shown E_c range are all backward peaking, again indicative of a rebound mechanism. Compared to the experimental distributions at $E_c \sim 12$ kcal mol^{-1}, the QCT distribution is somewhat broader. Considering the computed speed distributions we find that HB gives significantly broader distributions than 1GB and neither HB nor 1GB shows the experimentally observed small peak corresponding to $OD(v'=1)$. Nevertheless, the distributions at $E_c = 12$ kcal mol^{-1} show that both HB and 1GB reproduce well the maximum position of the main peak of the measured distribution.

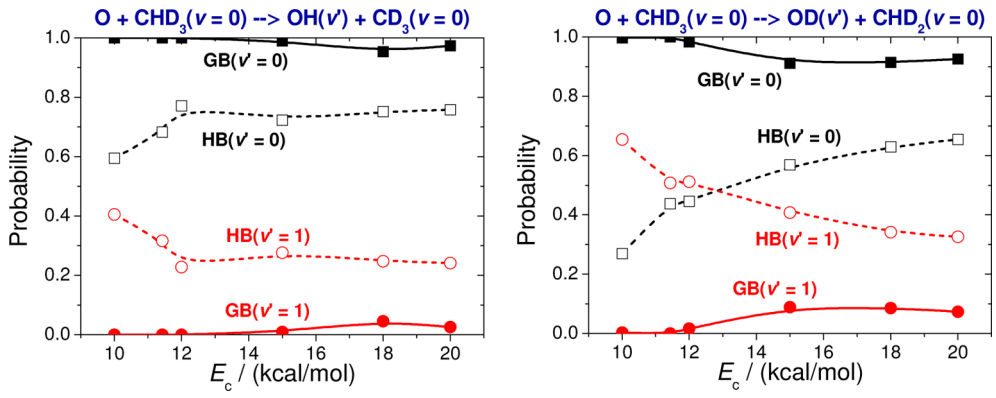

Figure 3. Computed correlated $OH(v')$ and $OD(v')$ vibrational branching ratios as a function of collision energy obtained by different binning techniques (HB and GB).

dx.doi.org/10.1021/jp510377k | J. Phys. Chem. A 2015, 119, 7190−7196

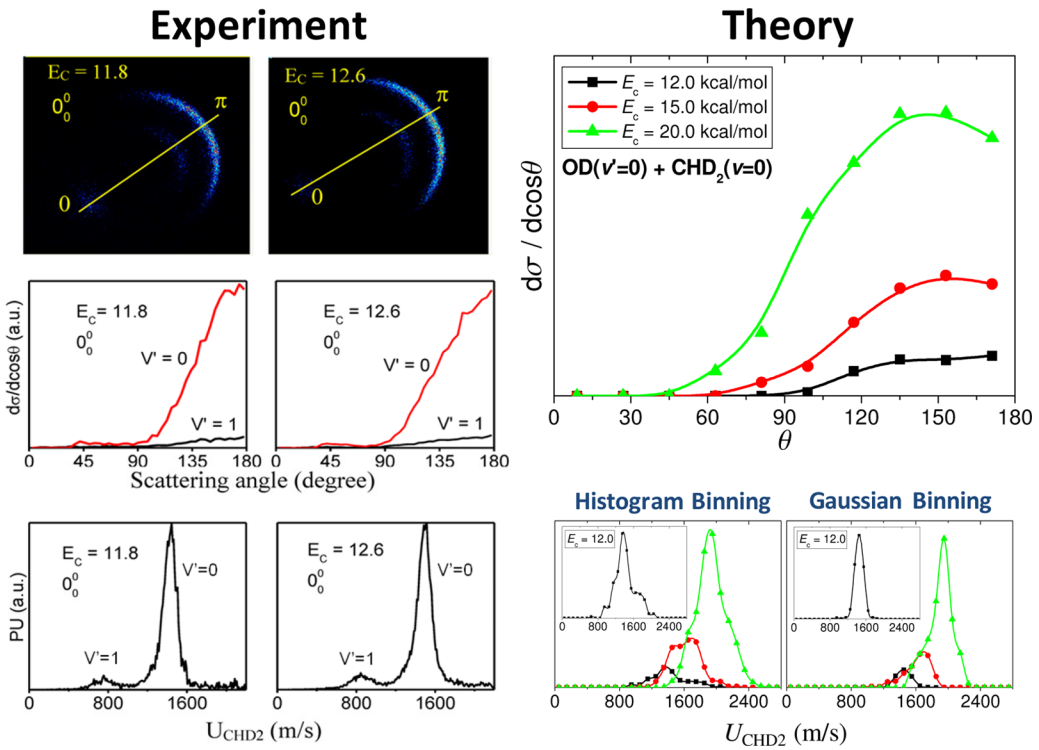

Figure 4. Upper experimental panel exemplifies two raw images of the $CHD_2(v=0)$ products. The two ring-like features in the backward hemisphere are ascribed to the concomitantly formed $OD(v'=0)$, the outer ring, and $OD(v'=1)$, the inner ring. The middle and lower experimental panels show the resultant correlated angular and product speed distributions, respectively. The computed correlated angular and $CHD_2(v=0)$ speed distributions at different collision energies are shown in the right panels. For the speed distributions histogram binning and Gaussian binning refer to the binning of the product vibrational states.

However, HB seriously overestimates the width of the $OD(v'=0)$ peak, whereas 1GB gives good agreement with experiment.

Figures 5 compares the experimental and theoretical excitation functions of the $OD(v')$ + $CHD_2(v=0)$ channels. As is the OH + CD_3 product channels, distinct concave-up shape in the post-threshold region is seen. HB-QCT and 1GB-QCT give similar concave-up excitation functions. As mentioned above, the main difference between the HB and 1GB results is that HB overestimates the $v' = 1$ cross sections relative to $v' = 0$, whereas 1GB gives good agreement with experiment. In the experimental panel the scale of the ordinate is normalized to that shown in Figure 2 by the relative signal strengths. Roughly speaking, the $CHD_2(v=0)$ signal is about a factor of 2 smaller than $CD_3(v=0)$, which deviates significantly from the QCT prediction, because the computed cross sections of $CHD_2(v=0)$ are 2−3 times larger than those of $CD_3(v=0)$. This discrepancy most likely arises from the unknown Frank−Condon factors of the two REMPI bands, $CD_3(0_0^0)$ versus $CHD_2(0_0^0)$, as well as the possible rotation-probe effects of the experiment.[42−44]

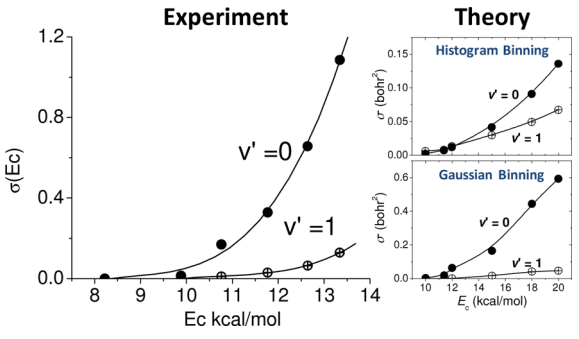

Figure 5. Experimental and theoretical excitation functions of the $OD(v')$ + $CHD_2(v=0)$ product channels. The yield of $OD(v'=0)$ is significantly higher than $OD(v'=1)$, suggestive of a vibrationally adiabatic pathway. The experimental scale of the ordinate is comparable to that for Figure 2, reflecting the relative REMPI signals in detecting the $CHD_2(v=0)$ and $CD_3(v=0)$ products. The QCT data are analyzed using different binning techniques. The absolute cross sections obtained by Gaussian binning (1GB) may not be realistic due to the normalization issue (see text for more details).

V. CONCLUSIONS

We report here a joint crossed-beam and QCT study of the $O(^3P)$ + $CHD_3(v=0)$ reaction over an extended E_c range. Three pair-correlated $CD_3(v=0)$ + $OH(v')$, $CD_3(v_2=2)$ + $OH(v')$ and $CHD_2(v=0)$ + $OD(v')$ product channels are examined. Qualitative or in some cases semiquantitative agreements between theory and experiment are found, from which a few general conclusions about the title reaction can be drawn. The underlying reaction mechanism is a direct rebound pathway, as suggested by the backward-dominant angular distribution. The cone-of-acceptance near the barrier must be relatively small (i.e., a tight-bend transition state), as manifested by the concave-up excitation functions in the post-threshold region and the narrowness of product scattered angle ranges. The reaction proceeds vibrationally adiabatically and yields predominantly the ground vibration states of products. Interestingly, the same conclusion of vibrational adiabaticity was also drawn in the stretch-excited reactions of $O(^3P)$ +

dx.doi.org/10.1021/jp510377k | J. Phys. Chem. A 2015, 119, 7190−7196

$CHD_3(v_1=1)$[15] and $CH_4(v_3=1)$.[24] By way of contrast, although the ground-state reactions of Cl + $CHD_3(v=0)/CH_4(v=0)$ are vibrationally adiabatic,[41,45] a significant nonadiabaticity was noted in the stretch-excited reactions.[46,47]

AUTHOR INFORMATION

Corresponding Authors

*K. Liu. E-mail: kliu@po.iams.sinica.edu.tw.

*G. Czakó. E-mail: czako@chem.elte.hu.

Present Address

§Department of Biomedical Engineering, University of Texas at San Antonio, One UTSA Circle, AET 1.240, San Antonio, TX 78249, USA.

Notes

The authors declare no competing financial interest.

ACKNOWLEDGMENTS

This work was supported by Academia Sinica and the Minister of Science and Technology of Taiwan (MOST 102-2119-M-001). G.C. thanks the Scientific Research Fund of Hungary (OTKA, NK83583) and the János Bolyai Research Scholarship of the Hungarian Academy of Sciences for financial support.

REFERENCES

(1) Campbell, I. M. *Energy and the Atmosphere*; John Wiley & Sons Ltd.: London, 1977.

(2) Baulch, D. L.; Cobs, C. J.; Cox, R. A.; Frank, C. E. P.; Just, Th.; Ker, J. A.; Pilling, M. J.; Troe, J.; Walker, R. W.; Warnatz, J. Evaluated Kinetic Data for Combustion Modeling. *J. Phys. Chem. Ref. Data* **1992**, *21*, 411−752.

(3) Czakó, G.; Bowman, J. M. Reaction Dynamics of Methane with F, O, Cl, and Br on Ab Initio Potential Energy Surfaces. *J. Phys. Chem. A* **2014**, *118*, 2839−2864.

(4) Li, Y.; Suleimanov, Y. V.; Yang, M.; Green, W. H.; Guo, H. Ring Polymer Molecular Dynamics Calculations of Thermal Rate Constants for the $O(^3P) + CH_4 \rightarrow OH + CH_3$ Reaction: Contributions of Quantum Effects. *J. Phys. Chem. Lett.* **2013**, *4*, 48−52.

(5) Gonzalez-Lavado, E.; Corchado, J. C.; Suleimanov, Y. V.; Green, W. H.; Espinosa-Garcia, J. Theoretical Kinetics Study of the $O(^3P) + CH_4/CD_4$ Hydrogen Abstraction Reaction: The Role of Anharmonicity, Recrossing Effects, and Quantum Mechanical Tunneling. *J. Phys. Chem. A* **2014**, *118*, 3243−3252.

(6) Espinosa-Garcia, J.; Garciá-Bernáldez, J. C. Analytical Potential Energy Surface for the $CH_4 + O(^3P) \rightarrow CH_3 + OH$ Reaction: Thermal Rate Constants and Kinetic isotope Effects. *Phys. Chem. Chem. Phys.* **2000**, *2*, 2345−2351.

(7) Gonzalez-Lavado, E.; Corchado, J. C.; Espinosa-Garcia, J. The Hydrogen Abstraction Reaction $O(^3P) + CH_4$: A New Analytical Potential Energy Surface Based on Fit to Ab Initio Calculations. *J. Chem. Phys.* **2014**, *140*, 064310.

(8) Suzuki, T.; Hirota, E. Vibrational Distribution of CH_3 Produced by the Reaction of $O(^1D)$ Atom with CH_4. *J. Chem. Phys.* **1993**, *98*, 2387−2398.

(9) Sweeney, G. M.; Watson, A.; McKendrick, K. G. Rotational and Spin-Orbit Effects in the Dynamics of $O(^3P_j)$ + Hydrocarbon Reaction. I. Experimental Results. *J. Chem. Phys.* **1997**, *106*, 9172−9181.

(10) Lin, J. J.; Zhou, J.; Shiu, W.; Liu, K. State-Specific Correlations of Coincident Product Pairs in the F + CD_4 Reaction. *Science* **2003**, *300*, 966−969.

(11) Zhou, J.; Lin, J. J.; Shiu, W.; Liu, K. State- Correlation Matrix of the Product Pair from F + $CD_4 \rightarrow DF(v') + CD_3(0\ v_2\ 0\ 0)$. *Phys. Chem. Chem. Phys.* **2006**, *8*, 3000−3006.

(12) Liu, K. Product Pair Correlation in Bimolecular Reactions. *Phys. Chem. Chem. Phys.* **2007**, *9*, 17−30.

(13) Zhang, B.; Liu, K. How Active is the Bend Excitation of Methane in the Reaction with $O(^3P)$. *J. Phys. Chem. A* **2005**, *109*, 6791−6795.

(14) Zhang, J.; Liu, K. Imaging the Reaction Dynamics of $O(^3P) + CH_4 \rightarrow OH + CH_3$. *Chem.—Asian J.* **2011**, *6*, 3132−3136.

(15) Wang, F.; Liu, K. Enlarging the Reaction Cone of Acceptance by Exciting the C-H Bond in the $O(^3P) + CHD_3$ Reaction. *Chem. Sci.* **2010**, *1*, 126−133.

(16) Czakó, G.; Bowman, J. M. Dynamics of the $O(^3P) + CHD_3(v_{CH} = 0, 1)$ Reactions on an Accurate Ab Initio Potential Energy Surface. *Proc. Natl. Acad. Sci. U. S. A.* **2012**, *109*, 7997−8001.

(17) Liu, R.; Yang, M.; Czakó, G.; Bowman, J. M.; Guo, H. Mode-Selectivity for a "Central" Barrier Reaction: Eight-Dimensional Quantum Studies of the $O(^3P) + CH_4 \rightarrow OH + CH_3$ Reaction on an Ab Initio Potential Energy Surface. *J. Phys. Chem. Lett.* **2012**, *3*, 3776−3780.

(18) Czakó, G.; Liu, R.; Yang, M.; Bowman, J. M.; Guo, H. Quasiclassical Trajectory Studies of the $O(^3P) + CX_4(v_k = 0, 1) \rightarrow OX(v) + CX_3(n_1n_2n_3n_4)$ [X = H and D] Reactions on an Ab Initio Potential Energy Surface. *J. Phys. Chem. A* **2013**, *117*, 6409−6420.

(19) Czakó, G. Communication: Direct Comparison Between Theory and Experiment for Correlated Angular and Product-State Distributions of the Ground-State and Stretching-Excited $O(^3P) + CH_4$ Reactions. *J. Chem. Phys.* **2014**, *140*, 231102.

(20) Yan, W.; Meng, F.; Wang, D. Quantum Dynamics Study of Vibrational Excitation Effects and Energy Requirement on Reactivity for the O + $CD_4/CHD_3 \rightarrow OD/OH + CD_3$ Reactions. *J. Phys. Chem. A* **2013**, *117*, 12236−12242.

(21) Espinosa-Garcia, J. Quasi-Classical Trajectory Study of the Vibrational and Translational Effects on the $O(^3P) + CD_4$ Reaction. *J. Phys. Chem. A* **2014**, *118*, 3572−3579.

(22) Monge-Paiacios, M.; González-Lavado, E.; Espinosa-Garcia, J. Quasiclassical Trajectory Study of the Effect of Antisymmetric Stretch Mode Excitation of the $O(^3P) + CH_4(v_3=1) \rightarrow OH + CH_3$ Reaction on an Analytical potential Energy Surface. Comparison with Experiment. *J. Chem. Phys.* **2014**, *141*, 094307.

(23) Martinez, R.; Enriquez, P. A.; Puyuedo, M. P.; González, M. Dynamics of the $O(^3P) + CH_4 \rightarrow OH + CH_3$ Reaction is Similar to That of a Triatomic Reaction. *J. Phys. Chem. A* **2012**, *116*, 5026−5029.

(24) Pan, H.; Liu, K. Communication: Imaging the Effects of the Antisymmetric-Stretching Excitation in the $O(^3P) + CH_4(v_3=1)$ Reaction. *J. Chem. Phys.* **2014**, *140*, 191101.

(25) Polanyi, J. C. Some Concepts in Reaction Dynamics. *Acc. Chem. Res.* **1972**, *5*, 161−168.

(26) Lin, J. J.; Zhou, J.; Shiu, W.; Liu, K. Application of Time-Sliced Ion Velocity Imaging to Crossed Molecular Beam Experiments. *Rev. Sci. Instrum.* **2003**, *74*, 2495−2500.

(27) Zhang, B.; Shiu, W.; Lin, J. J.; Liu, K. Mode Correlation of Product Pairs in the Reaction OH + $CD_4 \rightarrow HOD + CD_3$. *J. Chem. Phys.* **2005**, *122*, 131102.

(28) Zhang, B.; Shiu, W.; Liu, K. Imaging the Reaction Dynamics of OH + CD_4. 3. Isotope Effects. *J. Phys. Chem. A* **2005**, *109*, 8989−8993.

(29) Ma, Z.; Liu, K. Collision-Induced Fine-Structure Transition of $O(^3P_2) \rightarrow O(^3P_{0,1})$ by He and H_2: Excitation Function and Branching Ratio. *Chem. Phys. Lett.* **1993**, *213*, 269−274.

(30) Ma, Z.; Liu, K.; Harding, L. B.; Komotos, M.; Schatz, G. C. Differential Cross Sections for Fine Structure Transitions in $O(^3P_2)$ + Ar Collisions. *J. Chem. Phys.* **1994**, *100*, 8026−8039.

(31) Hudgens, J. W.; DiGiuseppe, T. G.; Lin, M. Two Photon Resonance Enhanced Multiphoton Ionization Spectroscopy and State Assignments of the Methyl Radical. *J. Chem. Phys.* **1983**, *79*, 571−582.

(32) Zhou, J.; Lin, J. J.; Shiu, W.; Pu, S.-C.; Liu, K. Crossed-Beam Scattering of F + $CD_4 \rightarrow DF + CD_3(v_{NK})$: The Integral Cross Sections. *J. Chem. Phys.* **2003**, *119*, 2538−2544.

(33) Zhou, J.; Lin, J. J.; Liu, K. Mode-Correlated Product Pairs in the F + $CHD_3 \rightarrow DF + CHD_2$ Reaction. *J. Chem. Phys.* **2003**, *119*, 8289−8296.

(34) Zhou, J.; Lin, J. J.; Liu, K. Observation of Reactive Resonance in the Integral Cross Section of a Six-Atom Reaction: F + CHD_3. *J. Chem. Phys.* **2004**, *121*, 813−818.
(35) Czakó, G.; Bowman, J. M. Quasiclassical Trajectory Calculations of Correlated Product Distributions for the F + $CHD_3(v_1 = 0, 1)$ Reactions Using an Ab Initio Potential Energy Surface. *J. Chem. Phys.* **2009**, *131*, 244302.
(36) Czakó, G. Gaussian Binning of the Vibrational Distributions for the Cl + $CH_4(v_{4/2} = 0, 1) \rightarrow$ H + $CH_3Cl(n_1n_2n_3n_4n_5n_6)$ Reactions. *J. Phys. Chem. A* **2012**, *116*, 7467−7473.
(37) Bonnet, L.; Espinosa-García, J. The Method of Gaussian Weighted Trajectories. V. On the 1GB Procedure for Polyatomic Processes. *J. Chem. Phys.* **2010**, *133*, 164108.
(38) Sonnenfroh, D. M.; Liu, K. Number Density-to-Flux Transformation Revisited: Kinematic Effects in the Use of Laser-Induced Fluorescence for Scattering Experiments. *Chem. Phys. Lett.* **1991**, *176*, 183−190.
(39) Zhang, B.; Liu, K.; Czakó, G.; Bowman, J. M. Translational Energy Dependence of the Cl + $CH_4(v_b = 0, 1)$ Reactions: A Joint Crossed-Beam and Quasiclassical Trajectory Study. *Mol. Phys.* **2012**, *110*, 1617−1626.
(40) Shiu, W.; Lin, J. J.; Liu, K.; Wu, M.; Parker, D. H. Imaging the Pair-Correlated Excitation Function: The F + $CH_4 \rightarrow HF(v')$ + $CD_3(v = 0)$ Reaction. *J. Chem. Phys.* **2004**, *120*, 117−122.
(41) Nyman, G.; Zhou, J.; Zhang, B.; Liu, K. Crossed-Beam and Quantum Dynamics Studies of the Reaction Cl + CHD_3. *Isr. J. Chem.* **2007**, *47*, 1−9.
(42) Zhou, J.; Shiu, W.; Lin, J. J.; Liu, K. Rotationally Selected Product Pair Correlation in F + $CD_4 \rightarrow DF(v')$ + $CD_3(v = 0, N)$. *J. Chem. Phys.* **2004**, *120*, 5863−5866.
(43) Zhou, J.; Shiu, W.; Lin, J. J.; Liu, K. Rotationally Selected Product Pair Correlation: F + $CD_4 \rightarrow DF(v')$ + $CD_3(v_2$=0, and 2, N). *J. Chem. Phys.* **2006**, *124*, 104309.
(44) Wang, F.; Liu, J.-S.; Chang, Y.; Liu, K. Vibrational Enhancement Factor of the Cl + $CHD_3(v_1$=1) Reaction: Rotational-Probe Effects. *J. Phys. Chem. Lett.* **2013**, *4*, 323−327.
(45) Zhou, J.; Zhang, B.; Lin, J. J.; Liu, K. Imaging the Isotope Effects in the Ground State Reaction of Cl + CH_4 and CD_4. *Mol. Phys.* **2005**, *103*, 1757−1763.
(46) Yan, S.; Wu, Y.-T.; Zhang, B.; Yue, X.-F.; Liu, K. Do Vibrational Excitations of CHD_3 Preferentially Promote Reactivity Toward the Chlorine Atom? *Science* **2007**, *316*, 1723−1726.
(47) Yan, S.; Wu, Y.-T.; Liu, K. Tracking the Energy Flow Along the Reaction Path. *Proc. Natl. Acad. Sci. U. S. A.* **2008**, *105*, 12667−12672.